ADVANCED ENERGY MATERIALS
www.advenergymat.de

Three-Dimensional Nanostructured Indium-Tin-Oxide Electrodes for Enhanced Performance of Bulk Heterojunction Organic Solar Cells

Hyunah Kwon, Juyoung Ham, Dong Yeong Kim, Seung Jae Oh, Subin Lee, Sang Ho Oh, E. Fred Schubert, Kyung-Geun Lim, Tae-Woo Lee, Sungjun Kim, Jong-Lam Lee, and Jong Kyu Kim**

A three-dimensional indium tin oxide (ITO) nanohelix (NH) array is presented as a multifunctional electrode for bulk heterojunction organic solar cells for simultaneously improving light absorption and charge transport from the active region to the anode. It is shown that the ITO NH array, which is easily fabricated using an oblique-angle-deposition technique, acts as an effective antireflection coating as well as a light-scattering layer, resulting in much enhanced light harvesting. Furthermore, the larger interfacial area between the electrode and the active layer, together with the enhanced carrier mobility through highly conductive ITO NH facilitate transport and collection of charge carriers. The optical and electrical improvements enabled by the ITO NH electrode result in a 10% increase in short-circuit current density and power-conversion efficiency of the solar cells.

1. Introduction

Organic solar cells are promising candidates for future photovoltaic devices due to their many advantages including cost-effective manufacturability of large-area devices, light weight, and mechanical flexibility.[1] Because the bulk heterojunction (BHJ) structure, in which electron-donating and accepting materials are intermixed with nanoscale phase morphologies, has great merits over the planar heterojunction structure, the former is widely used as the active layer of organic solar cells. On the one hand, the nanoscale phase morphology has a strong advantage in the dissociation of photo-generated excitons located within the exciton diffusion length (≈10 nm) at very large-area donor/acceptor interfaces.[2–5] On the other hand, it has an inherent disadvantage in the transport of the dissociated charges due to long percolated paths towards electrodes,[1] thereby limiting the thickness of BHJ active layer to typically less than 200 nm while thicker active layers would be desirable for absorbing more light. This forces an unsatisfactory compromise with regards to the thickness of a BHJ active layer to find an acceptable balance between light absorption and charge transport.[6–10] Accordingly, it would be very beneficial to develop a new approach to enhance light absorption without increasing the active layer thickness, and in a similar manner, to enhance charge transport without sacrificing light absorption.

Many nanotechnology-based efforts have been made to improve either light absorption or charge transport: For enhanced light absorption, various nanostructures including metal nanoparticles,[11] nanogratings,[8] nanowires, and photonic crystals[12] were used to take advantages of their strongly enhanced light scattering,[11] plasmonic effects,[13,14] and photon recycling.[12,15–18] For enhanced charge transport properties, block copolymer, nanoimprint lithography, and nanostructured anodes have been studied, especially for attaining a balance between electron and hole mobilities.[19–25] However, since the overall performance of solar cells is determined by the two sequential processes of light absorption and charge transport, a new approach enabling a simultaneous improvement in both processes is highly desirable.

Here, we present a new approach enabling simultaneous improvements in light absorption and charge transport properties of BHJ organic solar cells by introducing a 3D indium tin oxide (ITO) nanohelix (NH) array that serves as a multifunctional electrode. We find that the ITO NH array, easily fabricated by using oblique-angle deposition (OAD) on a conventional ITO bottom electrode, creates new optical functionalities: an efficient light-scattering function and a strong antireflection (AR) function. In addition, the microstructural properties of the ITO NHs, which strongly affect the charge transport properties, are systematically investigated. We find that the optical and electrical improvements enabled by the ITO NH electrode result in a 10% improvement in power-conversion efficiency (PCE) of the BHJ solar cells.

H. Kwon, J. Ham, D. Y. Kim, S. J. Oh, S. Lee,
Prof. S. H. Oh, K.-G. Lim, Prof. T.-W. Lee, Dr. S. Kim,
Prof. J.-L. Lee, Prof. J. K. Kim
Department of Materials Science and Engineering
Pohang University of Science and Technology
Pohang, 790–784, South Korea
E-mail: jllee@postech.ac.kr; kimjk@postech.ac.kr
Prof. E. F. Schubert
Department for Electrical
Computer, and Systems Engineering
Rensselaer Polytechnic Institute
Troy, NY, 12180, USA

DOI: 10.1002/aenm.201301566

2. Results and Discussion

2.1. Fabrication of the ITO NH Solar Cell Device

Figure 1 schematically shows the fabrication process of a BHJ solar cell with a three-dimensional ITO NH electrode. OAD technique was used to fabricate the ITO NH array, as shown in Figure 1a. At the initial stage of OAD, the obliquely incident ITO vapor flux produces small islands of deposited ITO material, behind which the vapor flux cannot reach due to a shadowing effect. This shadowing effect, along with limited adatom diffusion into shadowed areas and preferential deposition of the ITO vapor flux onto the non-shadowed regions, causes the film to grow by means of slanted nanorods. By controlling the substrate rotation speed (φ) together with the adjustable vapor flux incidence angle (θ), a variety of 3D nanostructures can be fabricated including straight nanorods, zigzag nanorods, and NHs. These sophisticated nanostructures can be made of virtually any evaporable materials (including ITO, SiO_2, TiO_2, and metals) in a simple, reproducible, and cost-effective way.[26,27] In the present study, the ITO NH arrays with various thicknesses, 100, 200, and 300 nm, were deposited by OAD on an ITO-coated glass substrate (see Figure 1b) for BHJ solar cells fabrication, followed by rapid thermal annealing for crystallization. After a poly(3,4-ethylenedioxythiophene):poly(styrenesulfonate) (PEDOT:PSS) hole-transport layer was spin-coated on the ITO NH array (Figure 1c), a poly(3-hexylthiophene (P3HT):[6,6]-phenyl-C61-butyric acid methyl ester (PCBM) blend active material was spin-coated (Figure 1d). Figure 1e shows a cross sectional scanning electron microscopy (SEM) image of the ITO NH array in which the spun-on PEDOT:PSS hole-transport and P3HT:PCBM active materials fills up the pore spaces between the NHs. Finally, a LiF/Al cathode contact was deposited using a thermal evaporator (Figure 1f). The thickness values of the active layers for the reference sample without NH array and 100, 200, and 300 nm NH samples were measured to be 200, 287, 305, and 311 nm, respectively, by a surface profiler. Note that the distance between the top of the NH arrays and the LiF/Al cathodes decreases with increasing the thickness of NHs because more infiltration of P3HT:PCBM active materials and higher porosity for thicker NHs, which may cause a large leakage current or short circuiting. (Supporting Information Figures S1–3)

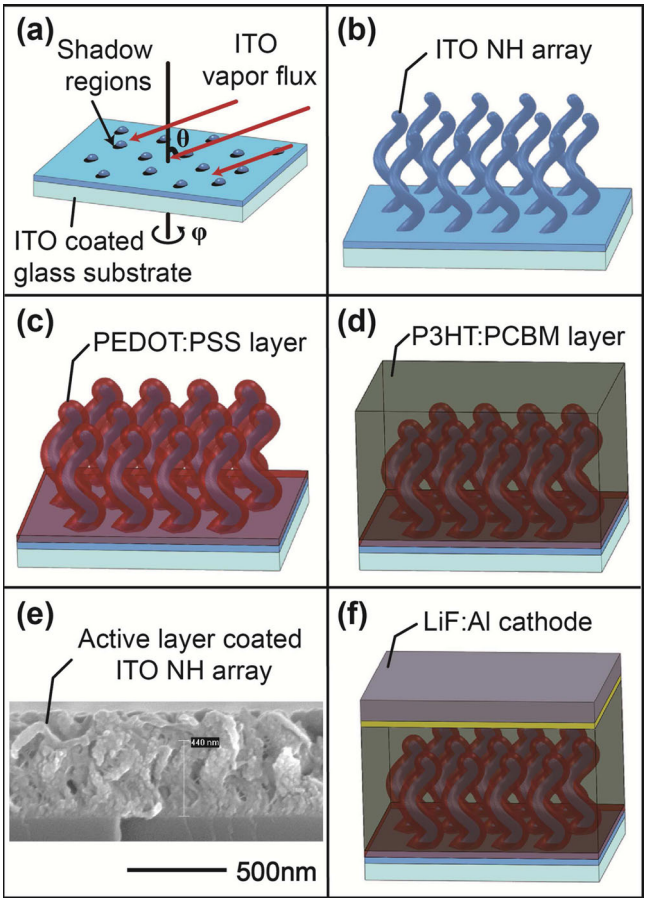

Figure 1. Fabrication process of a BHJ solar cell with the ITO NH electrode. a) Oblique angle deposition (OAD) process. By controlling θ (the vapor flux incidence angle) and φ (the substrate rotation speed), various 3D nanostructures can be fabricated including b) an array of ITO nanohelixes (NHs). c) PEDOT:PSS spin coating on the ITO NH array. d) P3HT:PCBM blend spin coating onto PEDOT:PSS coated sample. e) A cross-sectional SEM image of the ITO NH array on which PEDOT:PSS and P3HT:PCBM active materials are spun-on. f) LiF/Al cathode deposition.

2.2. Properties of the ITO NH Array

The transport of dissociated charges and their collection efficiency in BHJ solar cells is strongly influenced by the microstructural properties of the photoanodes, i.e., their ability to provide charges with an "express way" for efficient transport from the active region to the anode. Consequently, we investigated the microstructural properties of the ITO NH array by using SEM, X-ray diffraction (XRD), and transmission electron microscopy (TEM). **Figure 2**a shows a bird's eye view and a cross-sectional view (inset) SEM images of the ITO NH array fabricated by OAD. ITO NHs are randomly, yet quite uniformly distributed over the substrate surface, thereby forming a porous thin film. The porosity values of the NH arrays were estimated by using a linear effective medium approximation of refractive index values of the ITO NH arrays. The measured refractive indexes are 1.469 (100 nm NH array), 1.327 (200 nm NH array), and 1.238 (300 nm NH array), which correspond to porosities of 53%, 67%, and 76%, respectively (Supporting Information Figure S2). Such high porosity values indicate the existence of a high density of pores into which the active organic materials can easily penetrate during spin coating. Note that as the thickness of NH array increases, the porosity as well as the root-mean-square roughness increases (Supporting Information Figure S2), which may result in the increase of leakage current or the chance of short circuiting due to the spiky roughness (Supporting Information Figure S3)

Figure 2b shows XRD patterns of the ITO NH array before and after annealing. There is no diffraction peak for the as-deposited ITO NH, indicating that the as-deposited ITO NH array is in the amorphous state. After annealing the ITO NH array, diffraction peaks corresponding to crystallographic planes of the cubic (bixbyite type) ITO appear. Transmission

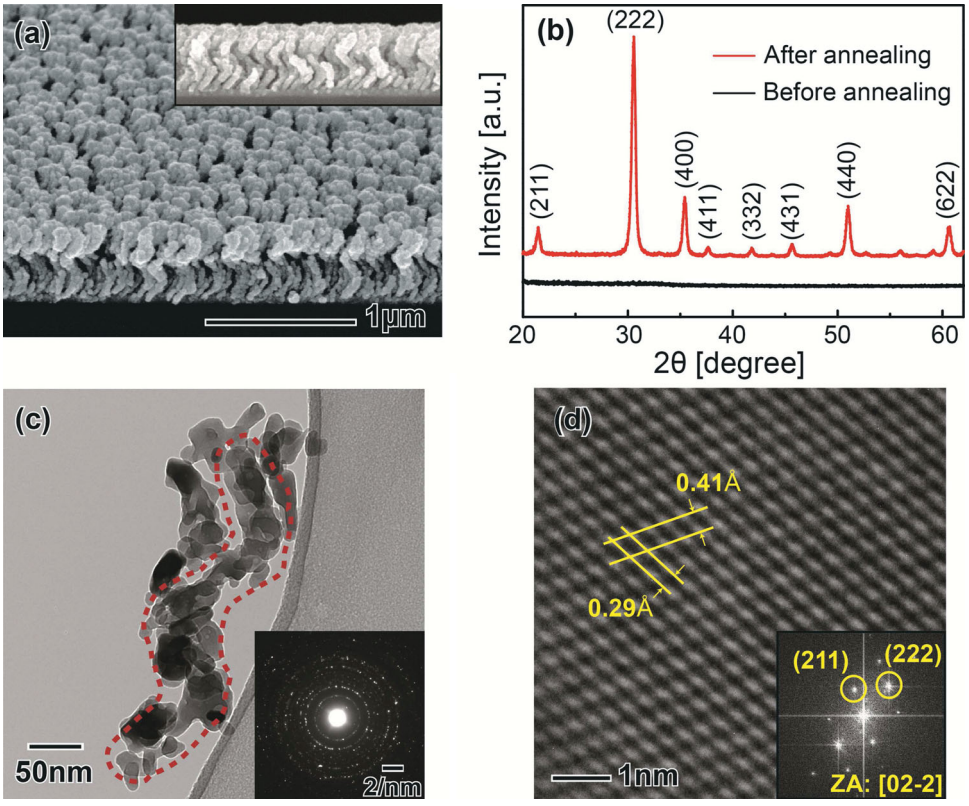

Figure 2. a) SEM bird's eye view and a cross sectional view (inset) of the ITO NH array after annealing to crystallize the ITO. b) XRD patterns of the ITO NH array before (black) and after (red) annealing. c) TEM image of an individual ITO NH. The inset shows the diffraction pattern from a bunch (group) of ITO NHs. d) HR-TEM image acquired from one of the grains shown in (c) and Fourier transformed diffraction pattern (inset).

electron microscopy (TEM) results including a diffraction pattern obtained from a group of ITO NHs are shown in Figure 2c. An ITO NH indicated by a red-dashed line consists of randomly oriented small crystalline grains. The polycrystalline structure of the ITO NH array was also confirmed by the diffraction pattern that consists of a series of rings, consistent with the XRD peaks. Figure 2d shows high-resolution TEM image acquired from one of the grains of Figure 2c; the TEM image shows clearly resolved lattice planes of (222) and (211) orientation whose d-lattice spacings are measured to be 0.29 Å and 0.41 Å, respectively. The Fourier transformed diffraction pattern was acquired from the same zone, which is indexed to the [02–2] zone axis pattern. Note that such an ITO NH electrode embedded in the BHJ active layer can facilitate the transport of dissociated charge carriers because it can provide a shorter travel distance for holes into the ITO electrode and a larger interface area between the ITO and the active materials. In the absence of the ITO NH, the hole transport path would be a percolated path, i.e., a potentially much longer path. Furthermore, once holes enter the ITO NHs, they can travel much faster through highly crystallized ITO NHs than through the P3HT:PCBM blend.

In addition to the change in electrical properties, it is expected that the formation of a porous ITO NH thin film onto an ITO/glass substrate can make a remarkable change in the optical properties particularly light scattering and transmittance in comparison with the ITO/glass substrate (not having an ITO NH array). Firstly, much enhanced light scattering by the 3D ITO NH array on ITO thin film is expected due to the increased hetero-interface area between the curled ITO NHs and the active material, which causes the propagating light to reflect, refract, and scatter. Secondly, an ITO NH film can act as an AR coating due to its intermediate refractive index that has a value between that of dense ITO and air (or the organic active layer); as a consequence, the optical reflection loss is reduced. Note that the ITO NH array on the ITO bottom electrode creates new optical functionalities. In addition to its intrinsic electrical transport function, an efficient light scattering function and an AR coating function are enabled, both of which are crucial for improving the light harvesting efficiency of solar cells. To prove our expectation, both scattering and AR effects were systematically investigated by performing simulations and experiments with ITO NH array solar cells.

To investigate light scattering effect of the ITO NH arrays, finite element method was carried out using software (COMSOL, Multiphysics). The simulated systems were the reference structure (P3HT:PCBM active layer on ITO thin film) and the ITO NH structure (ITO NH on ITO thin film surrounded by P3HT:PCBM). The refractive indices of ITO and the P3HT:PCBM active layer at the wavelength of 550 nm are 1.95 and 1.70, respectively. In the simulation, the electric field distribution without the ITO NH is calculated to be used as the background electric field for calculating the scattered field distribution when the ITO NH exists in the simulation structure.

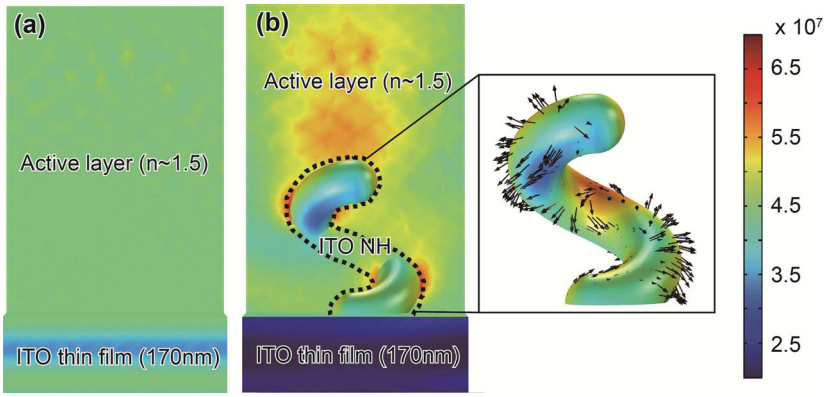

Figure 3. Simulated total electric field (V m^{-1}) distribution of a) the reference structure and b) the ITO NH structure. Panel (b) also shows the direction (black arrows) of the scattered field distribution at the surface of the ITO NH.

Figure 3a shows the simulated electric field (V m^{-1}) distribution in the reference structure. The magnitude of the electric field is indicated by the color scale on the 2D cross section planes cutting the center of the NH along the *z*-direction. Figure 3b presents the simulated electric field distribution in the ITO NH structure, showing more randomly and dynamically distributed field than the reference structure; the electric field enhancement is attributed to a strong light scattering effect caused by the 3D NH structure. Figure 3b also shows the amplitude (using a color scale) and the direction (using black arrows) of the electric field distribution at the surface of the ITO NH. The dynamic change of colors at the surface of the ITO NH and the randomly directed length-normalized arrows indicate the remarkable light scattering enabled by the ITO NH array structure.

To investigate the AR effect of the ITO NH arrays, optical transmittance curves of the ITO/glass substrate and the ITO NH arrays with various thicknesses (100, 200, 300 nm) on ITO/glass substrates were measured. To measure the transmittance, monochromatic light was incident from the glass substrate side and both transmitted and scattered lights were collected using an integrating sphere as illustrated in the inset of **Figure 4**a. Figure 4a,b show the measured and calculated transmittance curves, respectively, of the ITO/glass substrate (as indicated by black dotted lines) and the ITO NH arrays on ITO/glass substrate (as indicated by colored solid lines). Note that the calculated transmittance curves are consistent with the measured ones. The ITO NH arrays show much higher transmittance values in all cases, compared to the reference structure, in the wavelength range from 400 nm to 600 nm where P3HT:PCBM absorption band exists. Especially notable is that the 100 nm-thick ITO NH array shows the highest transmittance; this is because the 100 nm-thick NH layer, which has refractive index of 1.469, satisfies the AR coating condition of quarter-wavelength thickness in the range of visible light.[28] Note that the increase in transmittance is due to the reduced reflection loss enabled by the AR function of the ITO NH array on the ITO thin-film. Based on both calculated and measured transmittance data, we expect that the 100 nm-thick ITO NH array enhances the light absorption when used for photoanodes in BHJ solar cell devices.

Both the AR and light-scattering effects are important for enhancing the light absorption in the active layer. Therefore, the combined effect of the AR coating and the light-scattering layer on light absorption in a BHJ solar cell was investigated experimentally. The test BHJ structures for the absorption measurements consist of photoanodes (the reference, and ITO NH arrays with different thicknesses) on ITO/glass substrates, spun-on blended P3HT:PCBM active layers, and Al cathodes. The active layer thickness was controlled to be same for the test BHJ structures in order to avoid a thickness-dependent change in absorption. The measurement configuration including an integrating sphere, a detector, and the BHJ structure mounted so that the glass side contacts the integrating sphere with a 7° tilt angle is described in the inset of **Figure 5**. Assuming that the Al cathode reflects 100% of the incident light, the absorption in the active layer was obtained by subtracting the portion of reflected light (%) detected by the integrating sphere from the incident light (100%). Figure 5 shows the estimated absorption by the BHJ active layer with the reference ITO thin film and the ITO NH arrays as photoanodes. The BHJ structures

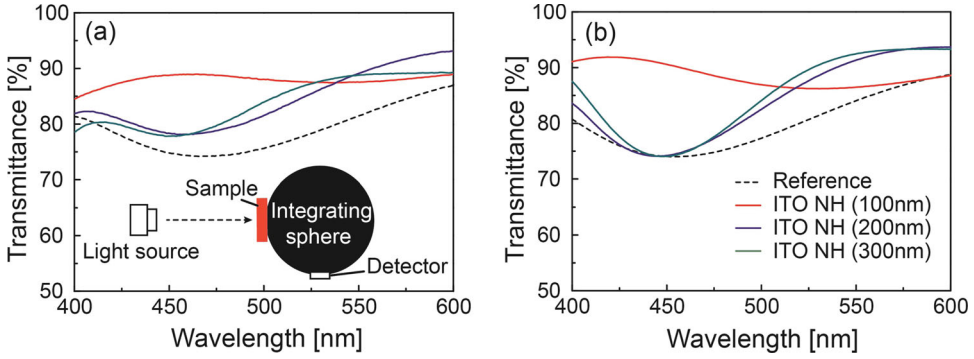

Figure 4. a) Measured transmittance versus wavelength of the reference structure (ITO thin film) (dotted line) and the ITO NH structures (100 nm: red, 200 nm: blue, 300 nm: green line). The optical measurement configuration using an integrating sphere is shown in the inset. b) Calculated transmittance versus wavelength of each structure.

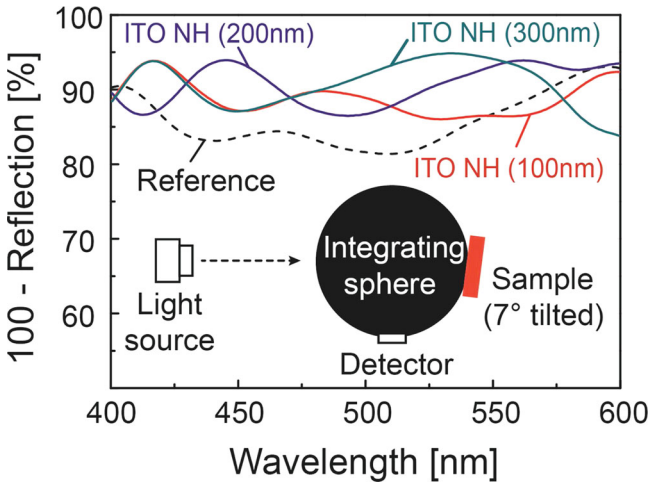

Figure 5. Measured light absorption by the BHJ active layer; the reference structure with ITO thin film photoanode (dotted line) and with various-thickness ITO NH photoanodes (100 nm: red, 200 nm: blue, 300 nm: green). The inset shows the measurement configuration with an integrating sphere. The BHJ structure was attached with the glass side contacting the opening of the integrating sphere with a 7° tilt angle.

with the ITO NH arrays show much higher absorption than the reference, in the wavelength range of the P3HT:PCBM absorption. The enhanced light absorption is attributed to the enhanced AR effect as well as light scattering by the 3D NH arrays. Even though the 100 nm-thick ITO NH array showed the highest transmittance in Figure 4, the thicker ITO NH arrays showed slightly more enhancement in light absorption in the overall wavelength range, indicating that the thicker ITO NH arrays have a stronger light scattering effect.

2.3. Device Performance

Figure 6a shows the current density–voltage (J–V) characteristics of BHJ solar cells with ITO NH arrays and typical planar photoanodes. Averaged solar cell performances acquired from the J–V curves are summarized in **Table 1**. The cell performance was enhanced for the 100 nm-thick ITO NH structure compared to the reference structure. However, thicker ITO NH structures showed a lower performance. The short circuit current density (J_{SC}) increased by 10% from 8.92 mA cm^{-2} to 10.04 mA cm^{-2} for the 100 nm-thick ITO NH array, corresponding to a 10% enhancement in PCE, from 3.31% to 3.62%. Open-circuit voltages of the 100 nm-thick ITO NH structure and the reference structure are very similar, indicating the PEDOT:PSS hole transport layer coated and surrounded the ITO NHs array very well. In addition, the J–V fill factors of both structures are comparable to each other even though the 100 nm ITO NH cell shows a higher dark leakage current than the reference cell (Supporting Information Figure S4). On the other hand, as the thickness of the NH layers increases to 200 nm and 300 nm, J–V curves shows reduced J_{SC} values, very large deviation from their average curves, and reduced parallel resistances, thus, reduced fill-factors, as summarized in

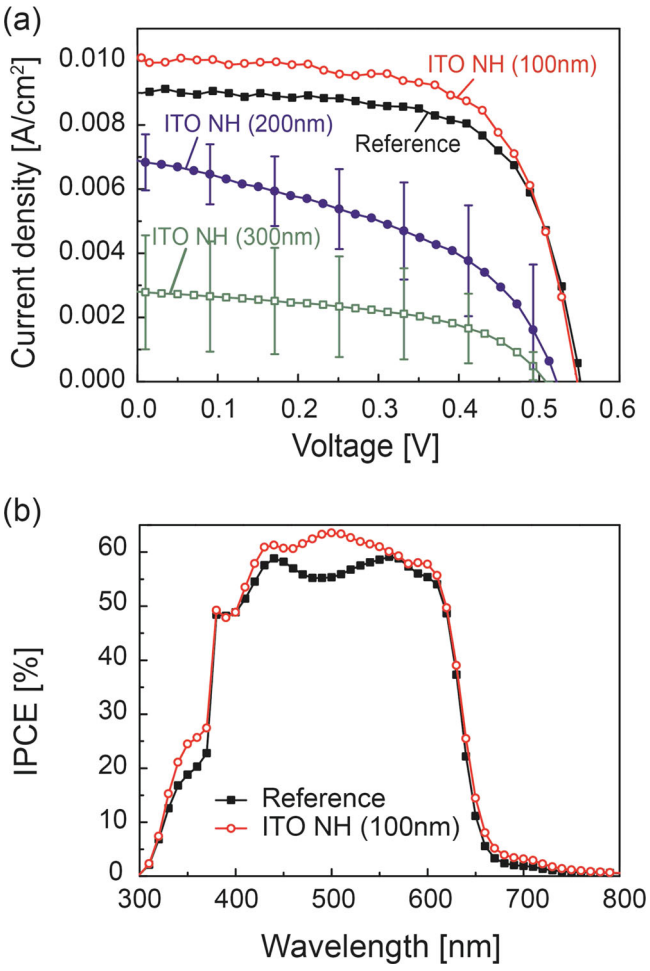

Figure 6. a) J–V characteristics of BHJ solar cells; the reference cell with typical planar photoanode (black line with squares) and with various-thickness ITO NH photoanodes (100 nm: red, 200 nm: blue, 300 nm: green line). b) Measured IPCE of BHJ solar cells with 100 nm ITO NH arrays and typical planar ITO photoanode as a function of the wavelength of incident light.

Table 1. We believe that the reason why the thicker ITO NH structures (200 nm and 300 nm thick) have lower performances than the reference and the 100 nm NH structures in spite of enhanced light absorption is as follows: the increase of the height of NH array results in i) increased porosity, ii) rough surface morphology, and iii) reduced distance between the top of the NH arrays and the cathode, and consequently iv) increase in the probability of a large leakage current or short circuiting.

Table 1. Performance measures of the reference cell and the ITO NH cell.

Performance measure	V_{OC} [mV]	J_{SC} [mA/cm^2]	Fill factor	PCE [%]
Reference cell	557.3	8.92	66.5	3.31
ITO NH cell (100 nm)	553.6	10.04	65.2	3.62
ITO NH cell (200 nm)	521.8	6.90	46.1	1.66
ITO NH cell (300 nm)	508.8	2.79	49.0	0.70

(Supporting Information Figure S1–3). We believe that the disadvantage of using thick NH arrays can be minimized, or even eliminated by an optimization of active-layer coating process.

The incident-photon-to-current-conversion efficiency (IPCE), defined by the ratio of the number of charge carriers collected by the solar cell to the number of photons of a given energy shining on the solar cell, was measured under the short-circuit condition. Figure 6b shows the measured IPCE of BHJ solar cells with 100 nm ITO NH array and reference planar ITO photoanode as a function of the wavelength of incident light. The ITO NH cell shows higher IPCE values than the reference cell in the wavelength range from 400 nm to 600 nm where the P3HT:PCBM absorption band exists. As discussed in the transmittance data shown in Figure 4 and the absorption by the active layer shown in Figure 5, the enhanced IPCE of the ITO NH cell is mainly attributed to the favorable optical functions, i.e., the AR function causing less reflection loss and the improved light scattering effect, enabled by the 3D ITO NH array. The integral of IPCE curve measured under the air mass 1.5 of solar irradiance spectrum (incident light flux, $F(\lambda)$) over the wavelength range is the short circuit photocurrent density (J_{SC}), $J_{sc} = \int qF(\lambda)QE(\lambda)\mathrm{d}\lambda$, where q is the elementary charge and $QE(\lambda)$ is the quantum efficiency, which agrees well with the enhanced J_{SC} and PCE by using the ITO NH photoanode.

We believe that enhancement of J_{SC} and the PCE for the 100 nm-thick ITO NH structure is due to simultaneous improvement in light absorption and charge transport properties enabled by the unique properties of the 3D ITO NH photoanode. **Figure 7** is a schematic picture showing how the ITO NH array affects the optical and the electrical properties of the BHJ solar cells in comparison with typical ones. The incident light and absorbed light are indicated by yellow arrows, while light loss is indicated by red arrows. When light is incident on the device, unavoidable Fresnel reflection occurs at the interface between the photoanode and the active layer. The ITO NH electrode can function as AR layer resulting in less reflection loss, thus more light is transmitted into the active layer than for the typical planar electrode, as experimentally confirmed in Figure 4. In addition, the transmitted light can be strongly scattered by the ITO NH array, as shown in Figure 3, leading to much enhanced light harvesting. The AR-coating effect combined with the enhanced light-scattering effect enabled by the ITO NH array, promotes the light absorption in the active layer, as shown in Figure 5, consequently resulting in much increased J_{SC} and PCE.

Finally, we discuss the electrical properties of the ITO NH electrode. The reference cell, with a P3HT:PCBM blended active layer, suffers from percolated pathways for charge transport between the active layer and the anode, which is an inherent property of the BHJ structure. In the ITO NH cell, however, the ITO NH photoanode embedded in the active layer provides dissociated holes with a shorter, wider, more direct travelling path. Furthermore, the highly crystallized ITO NHs as analyzed in Figure 2, can produce an express way for holes because the conductivity of the NHs is much higher than that of the P3HT:PCBM blend. In order to investigate the effect of ITO NH arrays on the electrical properties of solar cells, hole-only devices using Au as the top electrode and P3HT as the active layer were fabricated and characterized using the space-charge limited current model.[29,30] The hole mobilities of the hole-only devices with the reference ITO film and with 100 nm-thick ITO NH array were estimated to be 1.35×10^{-8} m^2 V^{-1} s^{-1} and 1.77×10^{-8} m^2 V^{-1} s^{-1}, respectively. The hole mobility in P3HT active layer with the ITO NHs electrode is 24% higher than that with the planar ITO one, indicating an enhanced charge transport enabled by ITO NH arrays (Supporting Information Figure S5). Therefore, the ITO NH photoanodes enhance charge transport properties without reducing, rather even enhancing light absorption, as shown in Figure 5. The simultaneous improvements in the optical and electrical properties of the BHJ solar cells make ITO NH photoanodes a noteworthy and promising approach to strongly enhance the performance in BHJ solar cells.

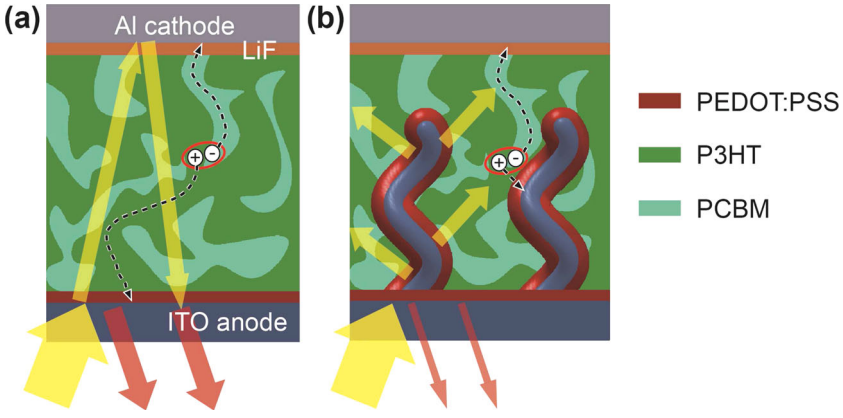

Figure 7. Schematic drawings of BHJ solar cells with a) a typical planar photoanode and b) an ITO NH photoanode. The incident light and absorbed light are indicated by yellow arrows and light loss (i.e., Fresnel reflection loss) is indicated by red arrows. Electrical paths of dissociated charge carriers are indicated by black dashed lines. a) In a reference cell, much more Fresnel reflection loss and less light scattering occur. Also dissociated charge carriers are collected into both contacts by means of long percolated pathways, resulting in a low charge collection rate. b) In an ITO NH solar cell, on the other hand, Fresnel reflection is much less due to the AR-coating effect of ITO NH array and due to stronger scattering of light entering from the ITO NH surface, resulting in enhanced light harvesting in the active layer. Furthermore, dissociated charge carriers, especially holes, can be collected more easily by the crystalline ITO NH array, resulting in an increased charge-carrier collection rate.

3. Conclusion

A 3D ITO NH array, easily fabricated by the OAD technique, was investigated for use as a multifunctional electrode in BHJ organic solar cells. It was found that the ITO NH array simultaneously improves light absorption and charge transport properties. The enhanced light absorption in the BHJ active layer is enabled by the ITO NH array due to its AR-coating effect and enhanced light-scattering effect. In addition, the embedded ITO NH photoanode facilitated the collection of dissociated charge carriers as well as hole transport from the active region to the anode. High crystallinity of the ITO NHs was found by XRD and TEM, implying a much higher conductivity of the

ITO NHs than P3HT:PCBM blended layer. Consequently, the BHJ organic solar cells coated with the 100 nm-thick ITO NHs electrode showed a 10% increase in J_{SC} and PCE compared with the conventional planar ITO electrode. The 3D metal-oxides NH electrodes have great potential to strongly improve the performance of various optoelectronic devices where both light absorption and electrical charge transport are important including photoelectrochemical cells and dye-sensitized solar cells.

4. Experimental Section

The ITO NH array was fabricated on an ITO-coated (170 nm) glass substrate using an electron-beam evaporator with the vapor flux incidence angle adjusted to 80°, the substrate rotation speed of 0.05 rpm, and the deposition rate of 2 Å s^{-1}. Subsequent to growth, the ITO NH array was annealed at 550 °C for 1 min at a pressure of 1.0×10^{-2} Torr. The ITO NH array was subjected to UV/O_3 treatment for 15 min using a power density of 30 mW cm^{-2} to make the ITO surface hydrophilic and amenable for uniform coating of polymer layers. ITO NH array samples were spin-coated with PEDOT:PSS (Clevios P VP AI 4083) at a rotation speed of 3000 rpm for 1 min, followed by annealing at 200 °C for 10 min. A P3HT:PCBM blend was prepared as follows: regioregular poly(3-hexylthiophene) (P3HT, Rieke Metals) was dissolved in 1,2-dichlorobenzene to make a 20 mg mL^{-1} solution, and phenyl-C_{61}-butyric acid methyl ester (PCBM, Nano-C) was blended at a 3:2 ratio. The blend was stirred for 14 h in a N_2-filled glove box (<0.5 ppm O_2 and H_2O). The prepared P3HT:PCBM blend was spin coated for 30 s on the PEDOT:PSS-coated samples in the glove box, using 700 rpm and 600 rpm for the reference cell and the ITO NH cell, respectively. For hole-only devices, only P3HT was spin coated for 30 s, using 500 rpm for both reference and 100 nm NH cells. Then the samples were dried for 10 min and annealed at 140 °C for 10 min. LiF/Al (1 nm/100 nm) and MoO_3/Au (10 nm/50 nm) were deposited by thermal evaporation at a base pressure 2×10^{-6} Torr for BHJ solar cell devices and hole-only devices, respectively.

Micro-tructural properties of the ITO NH array were characterized by using SEM (PHILPS XL30S), XRD (Rigaku D/MAX2500), and TEM (Jeol 2100F). Optical properties (transmittance and absorbance) were measured using a UV/VIS spectrometer (Perkin Elmer, Lambda 750S). For the light scattering simulation, COMSOL, a multiphysics engineering simulation software package, was used. The *J–V* characteristics of the solar cell device were measured in ambient air using a Keithley 2400 source measurement unit. The photocurrent was measured under AM 1.5G 100 mW cm^{-2} illumination using an Oriel 150 W solar simulator.

Supporting Information

Supporting Information is available from the Wiley Online Library or from the author.

Acknowledgements

The authors gratefully acknowledge support from the International Collaborative R&D Program funded by Korean Ministry of Knowledge Economy and Korea Institute for Advancement of Technology (KIAT), Global Research Network program (2011–220-D00064) and Basic Science Research Program through the National Research Foundation of Korea (NRF) funded by the Ministry of Education, Science and Technology (2009–0094036).

Received: October 15, 2013
Revised: December 3, 2013
Published online:

[1] H. Hoppe, N. S. Sariciftci, *J. Mater. Res.* **2004**, *19*, 1924.
[2] J. Halls, C. Walsh, N. Greenham, E. Marseglia, R. Friend, S. Moratti, A. Holmes, *Nature* **1995**, *376*, 498.
[3] G. Yu, A. J. Heeger, *J. Appl. Phys.* **1995**, *78*, 4510.
[4] S. H. Park, A. Roy, S. Beaupré, S. Cho, N. Coates, J. S. Moon, D. Moses, M. Leclerc, K. Lee, A. J. Heeger, *Nat. Photonics* **2009**, *3*, 297.
[5] Y. Kim, S. Cook, S. M. Tuladhar, S. A. Choulis, J. Nelson, J. R. Durrant, D. D. C. Bradley, M. Giles, I. McCulloch, C.-S. Ha, M. Ree, *Nat. Mater.* **2006**, *5*, 197.
[6] C. Cocoyer, L. Rocha, C. Fiorini-Debuisschert, L. Sicot, D. Vaufrey, C. Sentein, B. Geffroy, P. Raimond, *Thin Solid Films* **2006**, *517*, 511.
[7] K. S. Nalwa, J. M. Park, K. M. Ho, S. Chaudhary, *Adv. Mater.* **2011**, *23*, 112.
[8] S.-I. Na, S.-S. Kim, J. Jo, S.-H. Oh, J. Km, D.-Y. Kim, *Adv. Funct. Mater.* **2008**, *18*, 3956.
[9] M. Niggemann, M. Glatthaar, A. Gombert, A. Hinsch, V. Wittwer, *Thin Solid Films* **2004**, *451*, 619.
[10] X. Li, W. C. Choy, L. Huo, F. Xie, W. E. Sha, B. Ding, X. Guo, Y. Li, J. Hou, J. You, Y. Yang, *Adv. Mater.* **2012**, *24*, 3046.
[11] S. Hore, P. Nitz, C. Vetter, C. Prahl, M. Niggemann, R. Kern, *Chem. Commun.* **2005**, *15*, 2011.
[12] D.-H. Ko, J. R. Tumbleston, L. Zhang, S. Williams, J. M. DeSimone, R. Loqez, E. T. Samulski, *Nano Lett.* **2009**, *9*, 2742.
[13] V. E. Ferry, J. N. Munday, H. A. Atwater, *Adv. Mater.* **2010**, *22*, 4794.
[14] M. G. Kang, T. Xu, H. J. Park, X. Luo, L. J. Guo, *Adv. Mater.* **2010**, *22*, 4378.
[15] H. A. Atwater, A. Polman, *Nat. Mater.* **2010**, *9*, 205.
[16] Q. Gan, F. J. Bartoli, Z. H. Kafafi, *Adv. Mater.* **2013**, *25*, 2385.
[17] M. Niggemann, M. Riede, A. Gombert, K. Leo, *Phys. Status Solidi A* **2008**, *205*, 2862.
[18] Q. Zhang, C. S. Dandeneau, X. Zhou, G. Cao, *Adv. Mater.* **2009**, *21*, 4087.
[19] X. He, F. Gao, G. Tu, D. Hasko, S. Huttner, U. Steiner, N. C. Greenham, R. H. Friend, W. T. Huck, *Nano Lett.* **2010**, *10*, 1302.
[20] M.-G. Kang, M.-S. Kim, J. Kim, L. J. Guo, *Adv. Mater.* **2008**, *20*, 4408.
[21] D. Chen, W. Zhao, T. P. Russell, *ACS Nano* **2012**, *6*, 1479.
[22] C. O'Dwyer, M. Szachowicz, G. Visimberga, V. Lavayen, S. B. Newcomb, C. M. Torres, *Nat. Nanotechnol.* **2009**, *4*, 239.
[23] A. L. Beaudry, R. T. Tucker, J. M. LaForge, M. T. Taschuk, M. J. Brett, *Nanotechnology* **2012**, *23*, 105608.
[24] D. A. Rider, R. T. Tucker, B. J. Worfolk, K. M. Krause, A. Lalany, M. J. Brett, J. M. Buriak, K. D. Harris, *Nanotechnology* **2011**, *22*, 085706.
[25] H. K. Yu, W. J. Dong, G. H. Jung, J.-L. Lee, *ACS Nano* **2011**, *5*, 8026.
[26] D. J. Poxson, F. W. Mont, M. F. Schubert, J. K. Kim, E. F. Schubert, *Appl. Phys. Lett.* **2008**, *93*, 101914.
[27] J.-Q. Xi, M. Ojha, J. L. Plawsky, W. N. Gill, J. K. Kim, E. F. Schubert, *Appl. Phys. Lett.* **2005**, *87*, 031111.
[28] E. Hecht, Optics, Addison-Wesley, Boston, MA **2001**.
[29] C. Melzer, E. J. Koop, V. D. Mihailetchi, P. W. M. Blom, *Adv. Funct. Mater.* **2004**, *14*, 865.
[30] M. Kim, J.-H. Kim, H. H. Choi, J. H. Park, S. B. Jo, M. Sim, J. S. Kim, H. Jinnai, Y. D. Park, K. Cho, *Adv. Energy Mater.* **2013**, DOI: 10.1002/aenm.201300612.